SUPPLEMENTARY INFORMATION

We provide further details of our simulations in support of the results reported in the main body of the Letter.

1 The SPH Treecode Gasoline

We have used the fully parallel, N-body+smoothed particle hydrodynamics (SPH) code GASOLINE to compute the evolution of both the collisionless and dissipative component in the simulations. A detailed description of the code is available in the literature[31]. Here we recall its essential features. GASOLINE computes gravitational forces using a tree–code[32] that employs multipole expansions to approximate the gravitational acceleration on each particle. A tree is built with each node storing its multipole moments. Time integration is carried out using the leapfrog method, which is a second-order symplectic integrator requiring only one costly force evaluation per timestep and only one copy of the physical state of the system. In cosmological simulations periodic boundary conditions are mandatory. GASOLINE uses a generalized Ewald method[33] to arbitrary order, implemented through hexadecapole.

SPH is a technique of using particles to integrate fluid elements representing gas[34,35]. GASOLINE is fully Lagrangian, spatially and temporally adaptive and efficient for large N. The version of the code used in this Letter includes radiative cooling and accounts for the effect of a uniform background radiation field on the ionization and excitation state of the gas. The cosmic ultraviolet background is implemented using the Haardt-Madau model[23], including photoionizing and photoheating rates produced by PopIII stars, QSOs and galaxies starting at $z = 9$. The assumption that reionization occurred at high z is consistent with the combination of the 3rd year WMAP results and the Gunn-Peterson effect in the spectra of distant quasars[36]. We use a standard cooling function for a primordial mixture of atomic hydrogen and helium at high gas temperatures, but we include the effect of metal cooling[8] and evolving gas metallicities below 10^4 K (the metallicity in dwarfs is indeed much lower than solar[37], with $-1 < [Fe/H] < -2$). The internal energy of the gas is integrated using the asymmetric

formulation, that gives results comparable to the entropy conserving formulation[38] but conserves energy better. Dissipation in shocks is modeled using the quadratic term of the standard Monaghan artificial viscosity[35]. The Balsara correction term is used to reduce unwanted shear viscosity[39].

In the simulations described in this Letter star formation occurs when cold gas reaches a given threshold density[40,41] typical of actual star forming regions (we used 100 amu/cm^3 in most runs and discuss the effect of a lower threshold in §5). SF then proceeds at a rate proportional to $\rho_{gas}^{1.5}$, i.e. locally enforcing a Schmidt law. The adopted feedback scheme is implemented by releasing energy from SN into the gas surrounding each star particle[41]. The energy release rate is tied to the time of formation of each particle (which effectively ages as a single stellar population with a Kroupa IMF). To model the effect of feedback at unresolved scales, the affected gas has its cooling shut off for a time scale proportional to the Sedov solution of the blastwave equation, which is set by the local density and temperature of the gas and the amount of energy involved. In the high resolution runs described in this study this translates into regions of $\sim$ 0.1 to 0.3 kpc in radius being heated by SN feedback and having their cooling shut off. At z $>$1 the affected gas has its cooling shut off for typically 5-10 million years. However, even during high z starbursts only a few per cent of the gas in the disc plane has a temperature T $>$ 40,000 Kelvin. The effect of feedback is to regulate star formation in the discs of massive galaxies and to greatly lower the star formation efficiency in galaxies with peak circular velocity in the 50 $<$ V$_c$ $<$150 km/s range[25]. At even smaller halo masses (V$_c$ $<$ 20-40 km/s) the collapse of baryons is largely suppressed by the cosmic UV field[25,42]. Other than the density threshold only two other parameters are needed, the star formation efficiency (ϵSF = 0.1) and the fraction of SN energy coupled to the ISM (eSN=0.4). Similar values have been used in previous works by this group[4]. However, here we slightly increased ϵSF from 0.05 to 0.1 to ensure a better normalization to the radial Schmidt law. We explored values of eSN as high as 0.6 and cooling shutoff times changing by a factor of a few, verifying that, in the mass range of this study, mass profiles and SF histories are relatively insensitive to longer (shorter) cooling shutoff timescales if a smaller (larger) fraction of SN energy is coupled to the ISM.

2 Initial Conditions: Cosmological volume and the adopted cosmology

At z = 0 the virial mass of the halos that we studied in this Letter are 3.5 (DG1) and 2.0 (DG2) $\times$ 10^{10} $M_{\odot}$ (the virial mass is measured within the virial radius R_{vir}, the radius enclosing an overdensity of 100 times the cosmological critical density). The halos were selected within a large scale, low resolution, dark matter only simulation run in a concordance, flat, Λ-dominated cosmology: $\Omega_0 = 0.24$, Λ=0.76, $h = 0.73$, $\sigma_8 = 0.77$, and $\Omega_b = 0.042$[10,43]. The size of the box, 25 Mpc, is large enough to provide realistic torques for the small galaxies used in this work. The power spectra to model the initial linear density field were calculated using the CMBFAST code to generate transfer functions.

3 Volume renormalization technique

The simulations described here require a large dynamical range, from sub-kpc scales to correctly describe the internal dynamics of the dwarf galaxies, to several tens of Mpc to include the effects of cosmic torques from the large scale structure. This is achieved by the volume renormalization (or "zoom in") technique[44]. From the z=0 output of the large scale simulation the regions of interest where each galaxy forms were identified and traced back to a Lagrangian sub region in the initial conditions. Then the initial conditions are reconstructed using the same low-frequency waves present in the low resolution simulation but adding the higher spatial frequencies. The power spectrum is realized by using Fast Fourier Transforms (FFTs) to determine displacements of particles from this grid. We use a particular technique that allows one to calculate high resolution FFTs only in the regions of the simulations were mass and force resolution need to be high. To reduce the number of particles and make the full N-Body + SPH simulation possible with the same cosmological context, we construct initial conditions where the mass distribution is sampled at higher resolution (less massive particles on a finer grid) and then more coarsely as the distance from the chosen object increases. Dark

matter particle masses in the high resolution regions are 1.6×10^4 $M_\odot$, and the force resolution, i.e., the gravitational softening, is 86 pc (more details in Table 1). In total, at z=0 there are 3.3×10^6 particles within the virial radius of galaxy DG1. For all particle species, the gravitational spline softening, $\epsilon(z)$, was evolved in a comoving manner from the starting redshift (z $\sim$ 100) until z=8, and then remained fixed at its final value from z=8 to the present. The softening values chosen are a good compromise between reducing two body relaxation and ensuring that disc scale lengths and the central part of dark matter halos will be spatially resolved. Integration parameter values were chosen according to the results of previous systematic parameter studies[45]. This technique achieves CPU savings of several orders of magnitude, since running the original volume at the same resolution of the central region would have required more than 30 billion particles. This method has been successfully used in a wide range of cosmological studies[4,25,46] that have shown how the assembly history of the "zoomed-in" objects is preserved when compared to the original version in the low resolution volume.

4 The Photometric and Kinematic Analysis

To properly compare the outputs from the simulation to real galaxies and make accurate estimates of the *observable* properties of galaxies, we used the Monte Carlo radiation transfer code *SUNRISE*[29,47] to generate artificial optical images (see Figure 1 and Supplementary Figure 2) and spectral energy distributions (SEDs) of the outputs of our run. *SUNRISE* allows us to measure the dust reprocessed SED of every resolution element of the simulated galaxies, from the far UV to the far IR, with a fully 3D treatment of radiative transfer. Filters mimicking those of the SDSS survey[48] are used to create mock observations. The 2D light profiles are then fitted as the superposition of a Sersic and an exponential component using the widely used program GALFIT[49]. Results were compared with a two component, radially averaged 1D routine developed by the authors, finding similar results.

The model galaxy rotation curves (Figure 3) were determined using the standard tilted-ring analysis[50] that is applied to galaxy observations. The idea behind this is to facilitate a

comparison between galaxy models and observations by deriving rotation curves for both using the same methods. The assumption is that a rotating disc galaxy can be described by a set of concentric rings. Each ring has a constant circular velocity and two orientation angles. The values of the ring parameters are determined from the observed radial velocities in a set of concentric elliptic annuli. For each ring we determine the intensity weighted velocity along the line of sight at each pixel on the annulus and compute the rotational velocity of the gas at each annulus. The method has been recently applied to model galaxies[51] to study the effect of systematic biases due to non circular motions in the measured rotation curves of real galaxies[52].

5 Resolution tests and cosmic variance

Recent work has highlighted the role of numerical resolution and different SF and feedback implementations in driving the structural properties of simulated galaxies and specifically their internal mass distribution[53,54,55]. To demonstrate the robustness of our results analyse one of our galaxies (DG1) at lower resolutions, and a different galaxy with a different merger history (DG2), but similar mass and halo spin ($\lambda \sim 0.05$[56]), and show that our key results are produced in these simulations a) independently of the assembly history of the parent halo, b) when the spatial and force resolution are sufficiently high and c) when SF is spatially resolved, meaning that it happens only in cold gas particles dense enough to be representative of star forming regions, i.e. with density higher than 100 atom/cm^3.

The parameters of the analysed galaxies are summarized in Table 1, where the galaxy described in the main section of the Nature Letter is DG1, its lower resolution versions using the same initial conditions are DG1MR and DG1LR, and a version using a lower density threshold (0.1 amu/cm^3) for star formation is DG1LT (it has the same resolution as DG1MR). DG1DM is a run using the same initial conditions but including only the dark matter component. DG2 has the same mass and spatial resolution as DG1. Each run was completed following the guidelines described in the Initial Conditions section. The structural properties of the galaxies are measured using techniques that mimic observations and are presented in Table 2.

As shown in Supplementary Figure 1, poor resolution and an inconsistent implementation of star formation affect the global mass distribution of galaxies, leading to overly dense central regions. The rotational velocities based on the local 3D potential (and assuming circular orbits) for different DG1 realizations and for DG2 are plotted in the left panel of Supplementary Figure 1. Convergence is apparent in DG1 and DG1MR (particles in the DG1MR run are 2.3 times more massive). DG2, which has a final mass slightly smaller than DG1, also has a velocity profile that keeps raising for several kpcs. As a further test, we verified that the DM only run (DG1DM) has a DM profile similar to what obtained in previous, similar simulations[57], with a central DM density proportional to r^{α}, with $\alpha \sim$ -1.3 The above result shows that in our high resolution simulations the mass distribution of the galaxies presented in this Letter is free from numerical effects.

Instead, the low resolution run DG1LR forms a galaxy much more centrally concentrated. This run adopts the *same* SF criteria and feedback scheme as the higher resolution counterparts, but uses 64 times less particles than DG1 (force resolution is also 4 times worse, 350pc). DG1LR has a flat, rather than rising rotation curve. As we have shown in previous works, its low resolution causes enhanced angular momentum loss in the baryonic component via a variety of numerical effects[53]. These numerical effects come from the low number of resolution elements and exist irrespective of the modeling of the ISM and of the threshold density used for star formation. Moreover, at the resolution of DG1LR, a single gas particle has the mass of a SF region ($10^{5-6}M_{\odot}$). As individual density peaks are unresolved, SF only happens at the very center of the galaxy, further increasing the final central density of baryons and DM.

Similarly, to show how resolution, details of SF and outflows specifically affect the DM density profile, the various realizations of DG1 and DG2 are shown in the right panel of Supplementary Figure 1. DG1, the main simulation described in the Nature Letter is in blue, while the medium resolution simulation is in red, again showing shallow central DM profiles and clear convergence at our maximum resolution. DG2 has a shallow profile as well. On the contrary, the dot dashed black line shows the steep central profile of DG1DM, the DG1 dark matter only simulation, and highlights the degree to which the DM profile is flattened by processes

connected to the baryonic component.

In our high resolution simulations, where $T_{min} \sim 500K$ we resolve the local Jeans length implied by the high density threshold with at least 2 SPH kernels, thus preventing artificial fragmentation[58] as visually evident in the top right panel of Figure 1, showing a smooth gaseous disc. In DG1LR the resolution would not be enough to resolve the local Jeans length at the high density threshold, but the large gravitational softening (larger than both the smoothing length and the Jeans length) has a dominant effect, suppressing artificial fragmentation, Hence none of our runs suffers from artificial fragmentation and any clumpiness present is to be regarded as physical.

It is important to highlight that the the mass distribution of galaxy DG2 is similar to DG1, as the rotation curve is linearly rising for several scale lengths and the DM profile shows a shallow central region of about one kpc in radius. In panels a and b of Supplementary Figure 2, we plot the face and edge on surface brightness maps of DG2, and the resulting *i*-band surface density profile in panel c. Clearly, the profile is a pure exponential all the way to the center. A two component fit gives B/D=0.01, and a fit with a Sersic profile yields an index of 1, corresponding to a pure exponential disc. At difference with DG1, DG2 has a quiet merging history with fewer major mergers and only very minor accretion events after $z\sim 1.5$, showing that the suppression of bulge formation and a flat central DM profile depend more on the strength of feedback rather then on cosmic variance and the details of the recent assembly history of a given galaxy.

6 Inhomogeneous ISM, the removal of low angular momentum gas and the expansion of the central DM distribution

Several analytical and numerical papers have highlighted the necessity of resolving a clumpy multi-phase ISM to achieve a realistic modeling of energy deposition in the central regions of galaxies. While using a variety of arguments, these works suggest that only in a clumpy ISM is it possible to a) transfer orbital energy from gas to the DM as dense clumps sink through dynamical friction or resonant coupling[8,16,21,22,59,60] and have b) efficient gas outflows[15,54]. In

Run	DM Part. Mass $M_\odot$	Gas Part. Mass $M_\odot$	Force Resol. (pc)	Redshift$_{LMM}$ z	Stellar Mass $M_\odot$	SF
DG1	1.6e4	3.3e3	86	1.	4.8e8	High Th.
DG1MR	3.7e4	7.8e3	116	1.	5.0e8	High Th.
DG1LR	1e6	2.1e5	350	1.	4.8e8	High Th.
DG1LT	3.7e4	7.8e3	116	1.	3.7e9	Low Th.
DG1DM	2e4	-	86	1.	-	-
DG2	1.6e4	3.3e3	86	2.	1.8e8	High Th.

Table 1: Summary of the main numerical parameters for each simulation described in §3 and §5. From left: DM and gas particle masses, force resolution, redshift of the last major merger, galaxy stellar mass at z=0 and the SF model adopted.The high resolution DG1 and DG2 galaxies have a total virial mass of 3.5 (2.0) 10^{10} $M_\odot$ respectively. They both have a λ spin parameter[56] of 0.05. The highest resolution version of DG1 has about 3.5 million particles within the virial radius.

turn, these outflows 1) suppress the formation of stellar bulges by removing negative or low angular momentum gas[7,15,16,21] and 2) make the central DM expand by suddenly reducing the total enclosed mass and reducing the DM binding energy[21]. However, none of the above works has simultaneously studied the formation of bulgeless galaxies and that of DM cores, even if they both are crucial properties of small galaxies.

In order to achieve a multi phase ISM numerical works agree that a minimal spatial resolution of about 100pc is required, and that SF has to be associated with dense regions with gas density ($\sim$ 100 amu/cm^3)[40,61]. Our simulations satisfy both conditions and unify the many proposed models that focused on different aspects of the problem to robustly demonstrate that energy transfer and subsequent baryon removal are concurrent and effective to create bulgeless galaxies with a shallow DM profile in a full cosmological setting.

To illustrate the clumpiness of the ISM in our simulations, Supplementary Figure 3 highlights the differences in the density distribution of the interstellar medium between the simulations DG1MR and DG1LT, by plotting the local gas density vs radius of each gas particle at a representative epoch of z=0.75. These two runs have the same mass and spatial resolution and adopt identical feedback schemes. They only differ in the way regions where SF happens are selected. In the "high threshold" runs (DG1,DG2 DG1MR and DG1LR) SF happens only in regions above a high gas density threshold (100 amu/cm^3, the horizontal red line in the left panel

of Supplementary Figure 3). The density peaks then correspond to isolated clumps of cold gas with masses and sizes typical of SF regions. The efficiency of SF, ϵSF, for these regions must be increased from 0.05 (LT) to 0.1 (HT) in order to match the observed normalization of SF density in local galaxies. However, due to the increased densities, at any given moment only a few regions are actively forming stars. These star forming regions get disrupted after the first SNe go off and only a small fraction of gas has been turned into stars. Feedback then creates an ISM with cold filaments and shells embedded in a warmer medium. This patchy distribution allows the hot gas to leave the galaxy perpendicular to the disk plane at velocities around 100 km/s. Rather than developing a clumpy ISM as in the "high threshold" case, SF in the "low threshold" scheme is spatially diffuse (Supplementary Figure 3). This means that SN energy is more evenly deposited onto the gas component, but less overall gas is effected by SN feedback due to the low densities in the SF regions. By monitoring where SN energy is deposited and where gas gets substantially heated at high instantaneous rates, we verified that in the "high threshold" case a larger mass of gas achieves temperatures higher than the virial temperature ($T_{vir} \sim 10^5$ K) per unit mass of stars formed than in the "low threshold" scheme. Since less mass is affected in the "low threshold" scenario, the outflows are weak compared to the "high threshold" case. By z=0 DG1LT has formed ten times more stars, most of them in the central few kpcs, causing strong adiabatic contraction of the DM component. Its light profile is consistent with a B/D ratio of 0.3, typical of much more massive galaxies and more concentrated than in real dwarfs.

We note that in the runs adopting the "high threshold" SF, feedback produces winds that are comparable in strength to those happening in real galaxies of similar mass. However, in our simulations the cold ISM is still only moderately turbulent ($\sim$ 10 km/s at z=0), consistent with observations[62], and the galaxies match the observed stellar and baryonic Tully Fisher relation[63], as the SF efficiency is regulated to form an amount of stars similar to that of real dwarf galaxies of similar rotation velocity.

Supplementary Figure 4 illustrates an essential property of the simulations presented in this Letter: outflows selectively remove low angular momentum gas from high redshift galaxies.

Run	M_i	$g-r$	SFR $M_\odot$/yr	$R_s\ i$ kpc	V_{rot} km/s	M_{HI}/L_B
DG1	-16.8	0.52	0.01	0.9	56	1.2
DG1MR	-16.9	0.54	0.02	0.9	55	1.0
DG1LR	-18.7	0.33	0.22	0.9	62	0.64
DG1LT	-19.4	0.40	0.38	1.3	78	0.11
DG2	-15.9	0.46	0.02	0.5	54	2.8

Table 2: Summary of the observable properties of the different dwarf runs. the SFR is in M$\odot$/yr, R_s is the disc scale length, V_{rot} is measured using the HI velocity field as $W_{20}/2$

The mean angular momentum of gas blown out of the virial radius of galaxy DG1 is plotted as a function of time (red triangles) and shown to be as much as ten times smaller than the mean angular momentum of all the baryons (blue) and dark matter (black) accreted at the same time and then retained within the virial radius of the galaxy at $z = 0$. As the central region of a galaxy is being assembled at z $>$ 1.5 its mass profile and angular momentum content is then directly affected. This scenario, that maximizes energy transfer to the DM and gas outflows in the regions that will become the center of the galaxy by z=0, is a natural consequence of the hierarchical assembly of galaxies in the CDM model.

The results described in the Letter confirm that energy transfer and subsequent gas removal in a clumpy ISM have the net effect of causing the central DM distribution to expand, while at the same time limiting the amount of baryons at the galaxy center. In Supplementary Figure 1 we quantify this flattening by showing that by the present time the DM central profile in galaxies DG1 and DG2 is well approximated by a power law with slope α in the -(0.5–0.7) range. These values of α are significantly flatter than in the collisionless control run and are in agreement with those of observed shallow DM profiles in dwarf galaxies[13,14,64]. This result also resolves the dichotomy between CDM predictions of cuspy profiles based on DM–only runs[46,57] and observations: neglecting the modeling of gas outflows suppresses the removal of DM matter from the galaxy center and makes the formation of shallow profiles impossible. The central concentration of mass in DG1LT, in which outflows are negligible (Supplementary Figure 1) and DM adiabatically contracts rather than expanding, results in the very steep inner rise of the rotation curve, followed by a steep decline. Such declining rotation curves are unre-

alistic in small galaxies and have long plagued hydrodynamical galaxy formation simulations. By looking at smaller, but well resolved halos formed in the high resolution region of our simulations (but outside the virial radius of the main galaxies) we verified that star forming galaxies with rotational velocity $V_{rot} \sim 30$ km/s also have shallow DM profiles, while even smaller dark galaxies (where SF was completely suppressed due to the gas heating by the cosmic UV field) have steep central DM profiles. This result confirms that gas outflows caused by SF feedback are the cause for the removal of low angular momentum gas and the formation of DM cores.

References

31. Wadsley, J., Stadel, J., & Quinn, T., Gasoline: a flexible, parallel implementation of TreeSPH. *New Astr.* **9**, 137-158 (2004)

32. Barnes, J., & Hut, P., A Hierarchical O(NlogN) Force-Calculation Algorithm. *Nature* **324**, 446-449 (1986)

53. Ding, H.-Q.,Karasawa, N. and Goddard, III, W. A. The reduced cell multipole method for Coulomb interactions in periodic systems with million-atom unit cells. *CPL*, **196**, 6 (1992)

53. Gingold, R.A. & Monaghan, J.J. Smoothed particle hydrodynamics: theory and application to non-spherical stars. *Mon. Not. R. Astron. Soc.* **181**, 375-389 (1977)

53. Monaghan, J.J., Smoothed particle hydrodynamics. *Annual. Rev. Astron, Astrophys.* **30**, 543-574 (1992)

53. Alvarez, M.A., Shapiro, P., Kyungjin A. & Iliev, I.T. Implications of WMAP 3 Year Data for Sources of Reionization. *Astrophys. J.* **644** L101-L104 (2006)

37. Mateo, M., Dwarf Galaxies of the Local Group. *Annual Review of Astronomy and Astrophysics*. **36**, 435-506 (1998)

53. Springel, V., & Hernquist, L. Cosmological smoothed particle hydrodynamics simulations: the entropy equation. *Mon. Not. R. Astron. Soc.* **333**, 649-664 (2002)

53. Balsara, D.S., von Neumann stability analysis of smoothed particle hydrodynamics: suggestions for optimal algorithms. *J.Comput. Phys.* **121** 357-372 (1995)

40. Tasker, E. J. and Bryan, G. L. The Effect of the Interstellar Model on Star Formation Properties in Galactic Disks. Astrophys. J.**673**, 810–831 2008.

53. Stinson, G. Seth, A. Katz, N. Wadsley, J. Governato, F. Quinn, T. Star formation and feedback in smoothed particle hydrodynamic simulations - I. Isolated galaxies MNRAS, **373**, (2006)

42. Hoeft, M., Yepes, G., Gottlöber, S. and Springel, V. Dwarf galaxies in voids: suppressing star formation with photoheating. Mon. Not. R. Astron. Soc.**371**, 401–414, 2006

43. Verde, L. et al. First-Year Wilkinson Microwave Anisotropy Probe (WMAP) Observations: Parameter Estimation Methodology. Astrophys. J. Supp. Ser., **148**, 195-211. (2003)

44. Katz, N. and White, S. D. M. Hierarchical galaxy formation - Overmerging and the formation of an X-ray cluster. Astrophys. J., **412**, 455-478. (1993)

45. Power, C., *et al.*,The inner structure of Lambda CDM haloes - I. A numerical convergence study. *Mon. Not. R. Astron. Soc.* **338**, 14-34 (2003)

46. Diemand, J., Kuhlen, M. and Madau, P. Formation and Evolution of Galaxy Dark Matter Halos and Their Substructure. Astrophys. J., **667** 859-877 (2007).

53. Jonsson, P., Groves, B. and Cox, T. J. High-Resolution Panchromatic Spectral Models of Galaxies including Photoionisation and Dust. astro-ph/0906.2156 (2009)

53. Adelman-McCarthy, J. K. et al.,The Fourth Data Release of the Sloan Digital Sky Survey,*ApJS*,**162**, 38-48 (2006)

53. Peng, C. Y., Ho, L. C, Impey, C. D. and Rix, H. W., Detailed Structural Decomposition of Galaxy Images, Astron.J., **124**, 266-293 (2002)

53. Begeman, K. G., H I rotation curves of spiral galaxies. I - NGC 3198 Astron. Astrophys., **223**, 47-60 (1989).

53. Rhee, G., Valenzuela, O., Klypin, A., Holtzman, J., and Moorthy, B., The Rotation Curves of Dwarf Galaxies: A Problem for Cold Dark Matter? Astrophys. J., **617**, 1059, 1076 (2004)

53. Oh, S.-H., de Blok, W. J. G., Walter, F., Brinks, E. and Kennicutt, R. C., High-Resolution Dark Matter Density Profiles of THINGS Dwarf Galaxies: Correcting for Noncircular Motions Astron.J., **136**, 276 (2008)

53. Mayer, L., Governato, F. and Kaufmann, T. The formation of disk galaxies in computer simulations *Advanced Science Letters* **1** 7-27 (2008).

54. Zavala, J. Okamoto, T. and Frenk,, C. S. Bulges versus discs: the evolution of angular momentum in cosmological simulations of galaxy formation. Astrophys. J.**387**, 364-370 (2008)

55. Scannapieco, C., Tissera, P. and White, S. D. M. Effects of supernova feedback on the formation of galaxy discs Mon. Not. R. Astron. Soc.**389**, 1137-1149 (2008).

56. Bullock, J., Dekel, A., Kolatt, T. S., Kravtsov, A. V., Klypin, A. A., Porciani, C. and Primack, J. R. A Universal Angular Momentum Profile for Galactic Halos. Astrophys. J., **555**, 240-257 (2001)

57. Springel, V., Wang, J., Vogelsberger, M., Ludlow, A., Jenkins, A., Helmi, A., Navarro, J. F, Frenk, C. S. and White, S. D. M. The Aquarius Project: the subhaloes of galactic haloes. Mon. Not. R. Astron. Soc., **391**, 1685–1711 (2008).

58. Bate, M. R. and Burkert, A., Resolution requirements for smoothed particle hydrodynamics calculations with self-gravity. Mon. Not. R. Astron. Soc.**288**, 1060-1072 (1997)

59. Tonini, C., Lapi, A. and Salucci, P. Angular Momentum Transfer in Dark Matter Halos: Erasing the Cusp. Astrophys. J., **649**, 591–598, 2006

60. El-Zant, A. A., Hoffman, Y., Primack, J., Combes, F., & Shlosman, I. Flat-cored Dark Matter in Cuspy Clusters of Galaxies Astrophys. J. Lett., **607**, L75, 2004

61. Saitoh, T. R., Daisaka, H., Kokubo, E., Makino, J., Okamoto, T., Tomisaka, K, Wada, K. and Yoshida, N. Toward First-Principle Simulations of Galaxy Formation: I. How Should We Choose Star-Formation Criteria in High-Resolution Simulations of Disk Galaxies? PASJ **60**, 667 (2008)

62. Walter, F., Brinks, E., de Blok, W. J. G., Bigiel, F., Kennicutt, R. C., Thornley, M. D. and Leroy, A. THINGS: The H I Nearby Galaxy Survey. Astron.J., **136** 810–2125 (2008)

63. Blanton, M. R., Geha, M. and West, A. A. Testing Cold Dark Matter with the Low-Mass Tully-Fisher Relation Astrophys. J., **682**, 861–873 (2008).

64. Flores, R. A., & Primack, J. R. Observational and theoretical constraints on singular dark matter halos Astrophys. J. Lett., **427**, 1–4, (1994)

7 Supplementary Notes

FG acknowledges support from HST GO-1125, NSF ITR grant PHY-0205413 (also supporting TQ), NSF grant AST-0607819 and NASA ATP NNX08AG84G. CBB acknowledges the support of the UK's Science & Technology Facilities Council (ST/F002432/1). PJ was supported by programs HST-AR-10678 and 10958 and by Spitzer Theory Grant 30183 from the Jet Propulsion Laboratory. We thank the computer resources and technical support by TERAGRID, ARSC, NAS and the UW computing center, where the simulations were run.

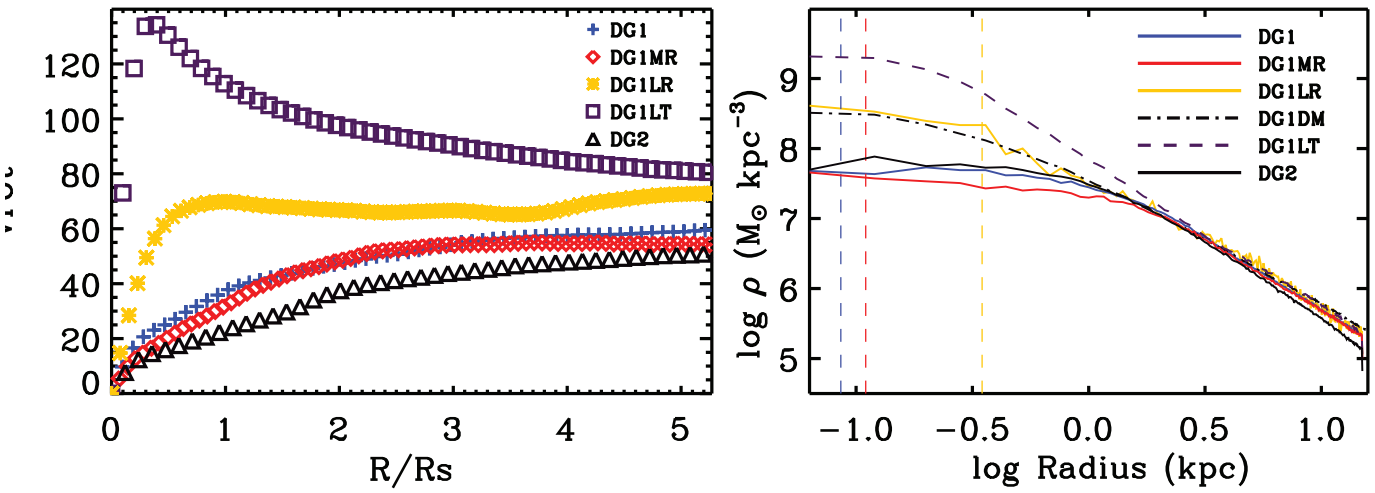

Figure 1: The rotation curve and DM radial distribution of the models described in §3 and §5, to show the effects of resolution and different SF recipes on the central mass distribution of simulated dwarf galaxies. The left panel shows the rotation curve, derived using the 3D potential of each galaxy and measured at z=0, for DG1 (blue crosses), DG1MR (red diamonds) and DG1LR, (yellow stars), plotted versus the disc scale length (1kpc for DG1, 0.5kpc for DG2). The three runs use the same gas density threshold for SF (100 atoms/cm^3), but MR and LR runs use only 40% and 12.5% of the particles of the reference run (with particle masses rescaled to the same total mass), and a softening respectively 1.33 and 4 times larger. Results have converged at the DG1MR resolution, while the LR run shows an excess of central material that is due to poor resolution causing artificial angular momentum loss[53]. The squares show DG1LT, where star formation is allowed in regions with a much lower local density (0.1 atoms/cm^3), again resulting in a much higher central mass density, due to the lack of outflows. This result demonstrates that the correct modeling of where SF is allowed to happen (namely only in gas with density comparable to that of real star forming regions) is crucial to obtain the results described in this Letter. The rotation curve of galaxy DG2 (black triangles) shows the same shape as that of the DG1 run. Panel B uses a similar colour scheme and plots the DM density profile for the same runs. DG1 (blue solid), DG1MR (red dashed) show similar profiles, with a DM core of about 1kpc. Color coded vertical lines mark the force resolution for each run. The DM only run DG1DM (dot dashed), shows instead a cuspy profile down to the force resolution (red dashed vertical line as for DG1MR). The central density is about 10 times higher than in the runs with strong outflows. DG2 has a similar profile to DG1, while the lower resolution run or the run with diffuse SF have dense and cuspy DM profiles down to the force softening length.

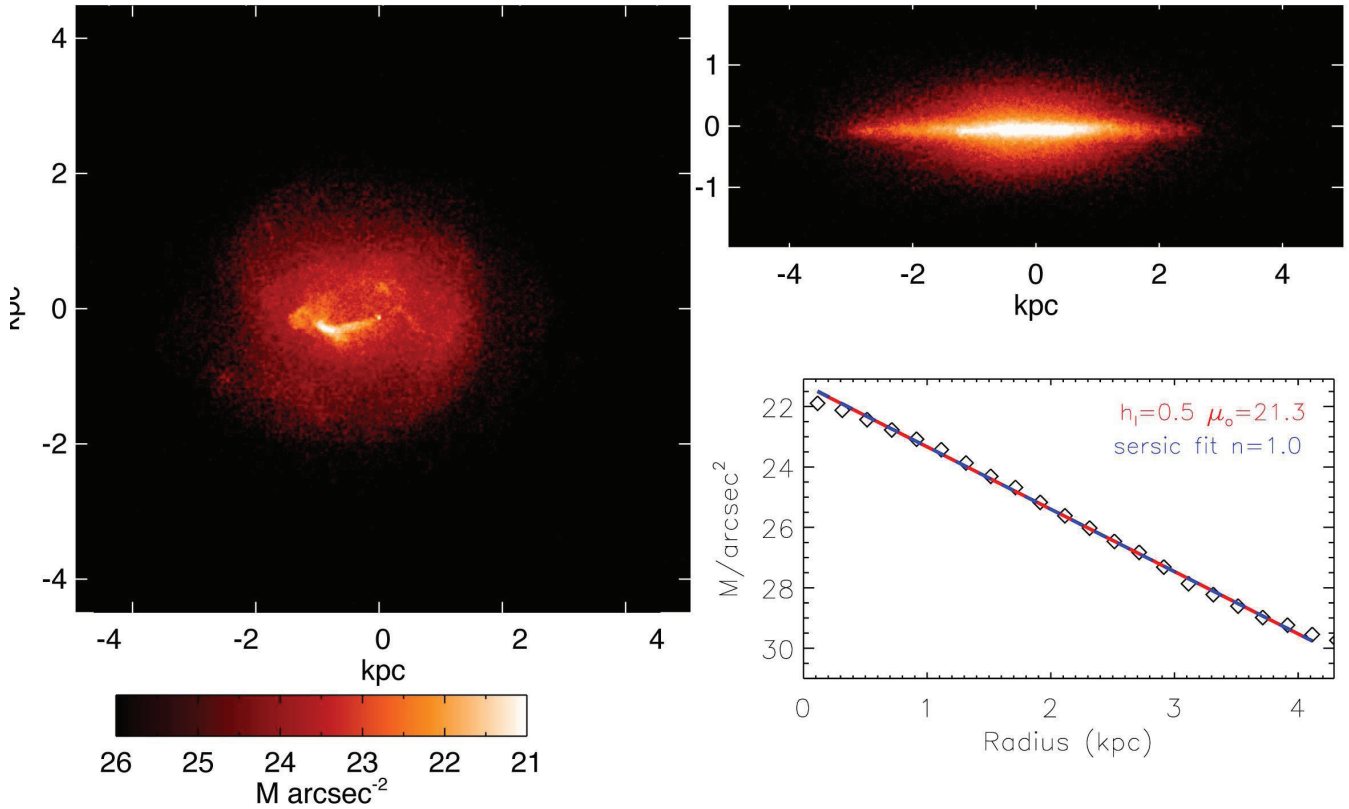

Figure 2: The optical properties of simulated galaxy DG2. Clockwise from left: The dust reddened i-band surface brightness map of galaxy DG2 seen face-on, edge-on, and the 1D radial surface brightness profile. The radial profile shows that the simulated galaxy is "bulgeless," with an almost perfect exponential profile with a scale length of 0.5 kpc. (the Sersic profile with n=1 is equivalent to an exponential profile).

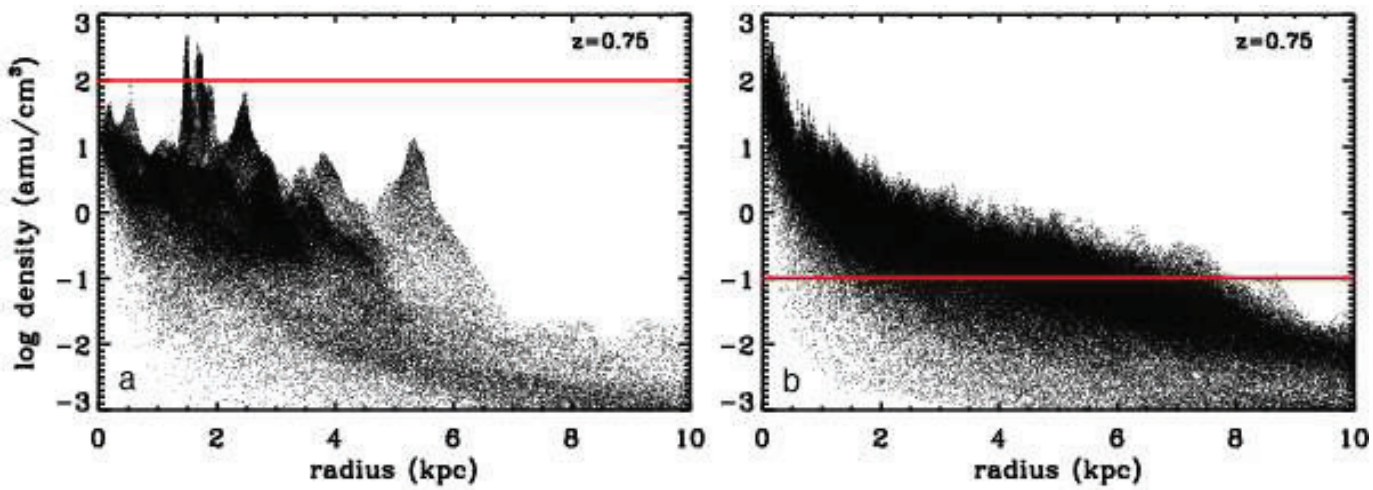

Figure 3: Properties of the gas distribution for different SF implementations. The local gas density measured around each SPH particle is plotted as a function of its radial distance from the galaxy center for runs DG1MR and DG1LT, which have identical force and mass resolution, but differ in the star formation density threshold. Horizontal red lines mark the minimum gas density for SF in each run. In both runs the SFR is $\propto {\rho_{gas}}^{1.5}$. In the low threshold simulation, diffuse star formation in the inner regions continues unabated by feedback, as SN energy is more evenly distributed and is unable to originate major outflows. Allowing star formation only in high density regions results in a complex, inhomogeneous ISM, even in the central regions and fast outflows that remove gas preferentially from the galaxy center.

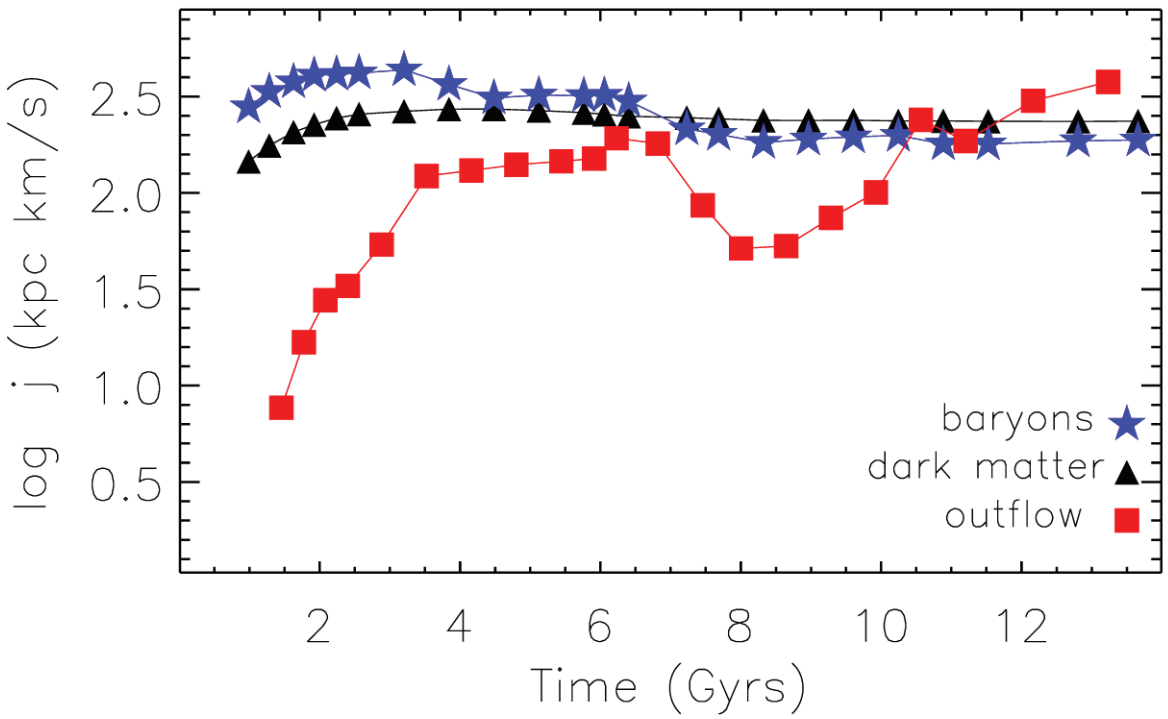

Figure 4: The angular momentum per unit mass of the DM and gas being accreted and of the gas being blown out as a function of time. While most of the matter accreted onto the galaxy halo has a fairly constant angular momentum, the gas being blown out at high redshift has a systematically lower angular momentum, by as much as an order of magnitude. During the same epoch and until z=1 the SFH of the galaxy is quite bursty. The stronger bursts are closely associated with epochs where the baryon distribution is clumpier and with decreases of the central DM density, supporting models[8,15] for the formation of the DM core and the formation of bulgeless galaxies.

8 Supplementary Movie Legend

The movie shows the evolution of the gas density (in blue) in the region where galaxy DG2 forms, from shortly after the Big Bang to the present time. The frame is 15 kpc per side. Brighter colors correspond to higher gas densities. The movie highlights the numerous outflows that remove low angular momentum gas and the connection between outflows with accretion and early merger events. Some of the mergers are with dark satellites and are not directly visible in the movie.